

# Corrosion Properties of Nanocrystalline Co–Cr Coatings

D. CHENG,<sup>1</sup> V. L. TELLKAMP,<sup>1</sup> C. J. LAVERNIA,<sup>2</sup> and E. J. LAVERNIA<sup>1</sup>

<sup>1</sup>Department of Chemical and Biochemical Engineering and Materials Science, University of California, Irvine, Irvine, CA and

<sup>2</sup>Department of Orthopedics and Biomedical Engineering, University of Miami, Miami, FL

(Received 31 March 2000; accepted 13 June 2001)

**Abstract**—Nanocrystalline and conventional Co–Cr (ASTM F75) coatings were prepared by plasma spraying for possible orthopedic implant applications. Scanning electron microscopy and transmission electron microscopy were used to study the macrostructure and microstructure of the resultant sprayed coatings. The corrosion resistance was characterized by an *in vitro* potentiodynamic anodic polarization technique in a pseudo-physiological solution. The nanocrystalline coating has higher porosity, lower corrosion current density, and less localized damage than that of the conventional one, demonstrating better application potential for orthopedic implants. A change in the atomic compositional difference between the grain interior and the grain boundary, the presence of residual strain in the grain interiors, and a change in the repassivation kinetics are discussed as possible explanations for the enhanced corrosion behavior observed. © 2001 Biomedical Engineering Society. [DOI: 10.1114/1.1397790]

**Keywords**—Localized damage, Grain boundaries, Plasma spraying, Anodic polarization.

## INTRODUCTION

Thermal sprayed coatings have been studied for application in medical fields, typically, in orthopedic and dental prostheses.<sup>4,13,21</sup> Conventional prostheses are made of bioinert materials such as Ti–6Al–4V alloys or CoCr-type alloys such as ASTM designated F75 alloys.<sup>21</sup> Thermal sprayed coatings lead to improvements in the material properties of the bearing surface, diminishing the wear of prosthetic devices.<sup>4</sup> For prosthetic applications, the coating must have a high hardness, high porosity, and good adhesion to the prosthesis.<sup>21</sup> Furthermore, thermal sprayed coatings must be biocompatible and remain mechanically stable following implantation.<sup>21</sup> Recently, thermal spraying of nanocrystalline coatings has attracted considerable scientific and industrial interest due to the reported improvements in the properties, such as increased hardness, strength, and ductility.<sup>3</sup> In a previous study, a nanocrystalline CoCr coating was success-

fully prepared by plasma thermal spraying and an increase in microhardness and porosity over the conventional counterpart was reported.<sup>16</sup> The objective of the present study is to investigate the corrosion behavior of a nanocrystalline CoCr coating for potential implant applications.

## EXPERIMENT

In the present study, gas atomized ASTM F75 Co-based superalloy powders, with an average particle size of 88  $\mu\text{m}$ , were mechanically milled in a methanol environment. The milled powders were then sprayed on Ti substrates by plasma spraying (Sulzer Metco 7M spray system) to generate nanocrystalline coatings. A detailed description of the process can be found elsewhere.<sup>16</sup> For the purpose of comparison, unmilled powders were also sprayed to obtain a conventional coating. The morphology of the as-sprayed coatings was observed using a Philips XL 30 FEG scanning electron microscopy (SEM). The grain size of the nanocrystalline powders and coating were determined by the dark-field technique using a Philips CM20 transmission electron microscope (TEM) operated at 200 keV. The milled powders to be analyzed by TEM were dispersed in methanol, deposited on carbon grid substrates, and allowed to dry in air. The TEM sample for the as-sprayed coating was prepared using dual-jet polishing. The average grain size of the nanocrystalline powders and coating were obtained by measuring and averaging at least 100 grains.

The density of the coatings was determined according to ASTM B328—standard test method for density, oil content, and interconnected porosity of sintered metal structural parts and oil-impregnated bearings. This technique compensates for the open surface pores of powder metallurgy parts when using the Archimedes method of determining density by first immersing the sample in oil to seal any surface pores. The sample is weighed in air as received. It is then submersed in oil in a vacuum retort at slightly higher than room temperature for a period of 4 h. The oil-impregnated sample is weighed in air. The oil-impregnated sample is next weighed in water

Address correspondence to E. J. Lavernia, Professor, Department of Chemical and Biochemical Engineering and Materials Science, University of California, Irvine, Irvine, CA 92697-2575. Electronic mail: lavernia@uci.edu

TABLE 1. Concentration of Hank's solution.

Chemicals	Concentration (g/l)
NaCl	8.00
CaCl <sub>2</sub>	0.14
KCl	0.40
NaHCO <sub>3</sub>	0.35
Glucose	1.00
NaH <sub>2</sub> PO <sub>4</sub>	0.10
MgCl <sub>2</sub> ·6H <sub>2</sub> O	0.10
Na <sub>2</sub> HPO <sub>4</sub> ·2H <sub>2</sub> O	0.06
MgSO <sub>4</sub> ·7H <sub>2</sub> O	0.06

by suspending the sample in water from a fine wire attached to the beam hook of a balance while the beaker of water is supported over the balance pan by a small bridge. Finally, the density of the sample is determined by

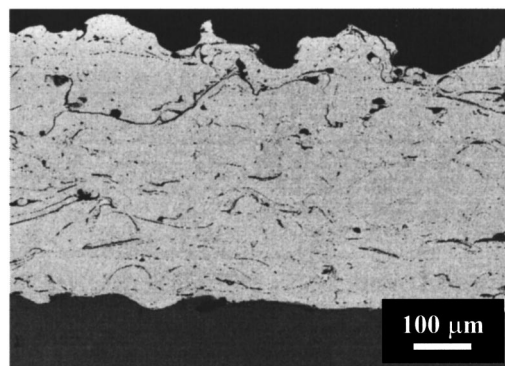
$$D = [A/(B - F)]D_w, \quad (1)$$

where  $A$  = the mass of the oil-free sample in air,  $B$  = the mass of the oil-impregnated sample weighed in air,  $F$  = the mass of the oil-impregnated sample weighed in water, and  $D_w$  = the density of water.

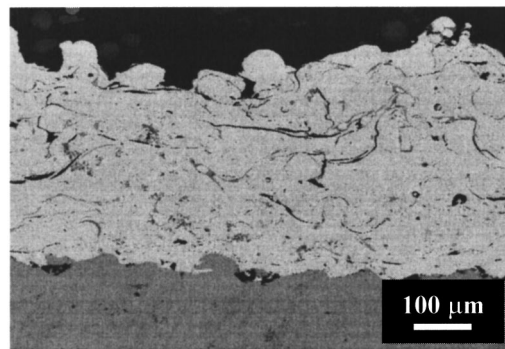
The corrosion behavior was studied using an electrochemical method that incorporates a computerized potentiostat. A single-compartment, three-electrode glass cell was employed along with a Pt wire as the counterelectrode and a saturated calomel electrode (SCE) as the reference electrode. The electrolyte was Hank's solution (composition shown in Table 1) and its pH was adjusted to  $7.00 \pm 0.05$  with sodium bicarbonate. Conventional and nanocrystalline CoCr-coated specimens were used as working electrodes. To eliminate the effect of surface roughness, the CoCr electrodes were polished to a mirror finish. The working electrodes were initially immersed in the solution to stabilize them for a period of 1 h and then the potential was scanned between  $-600$  and  $1500$  mV with a scanning rate of  $10$  mV/s for 130 cycles. Following the corrosion studies, the specimen surface morphology was observed by SEM.

## RESULTS AND DISCUSSION

Figure 1 shows the backscattered electron images obtained from the SEM analysis performed on the cross-section areas of the as-sprayed conventional (a) and nanocrystalline (b) coatings. No discernable macroscopic differences between the coatings are evident. Quantitative measurement of the density of the coatings was determined following ASTM B328. The porosity of the nanocrystalline coating was determined to be 9.6 vol% as compared to 4.5 vol% for the conventional coating; however, the reader should note that only one density



(a)



(b)

FIGURE 1. Cross-sectional backscattered SEM images of conventional (a) and nanocrystalline (b) coatings.

sample was measured for each coating. Several mechanisms have been recently proposed to explain the formation of pores during thermal spraying. The presence of porosity in thermal sprayed coatings is closely related to the thermal, fluid flow and solidification conditions that are present. As a result, the solidification of the impinging spray droplets on a substrate can be considered as a series of individual events: impingement, deformation, and solidification. Coating porosity depends on the pressure induced on the surface of the substrate during droplet impingement.<sup>24</sup> Studies have shown that porosity decreases with increasing particle velocity and increasing temperature.<sup>24</sup> A high droplet temperature before impingement, created by a short spraying distance, decreases the porosity level due to improved filling of cavities by the molten particles. The observed increase in porosity of the coating generated using nanocrystalline powders is thought to be attributed to the irregular morphology of the powders, which leads to a large volume fraction of interstitial cavities during impingement and deformation. This suggestion is consistent with available results from other investigations.<sup>15</sup> The porosity present in the nanocrystalline coatings is expected to influence the physical properties of the coatings.<sup>5,10,14,18,30</sup>

Figure 2 shows TEM bright-field, dark-field, and selected-area diffraction (SAD) pattern micrographs that reveal the grain size of the nanocrystalline CoCr powders prior to thermal spraying. Figure 3 shows the TEM bright-field, dark-field, and SAD pattern micrographs that reveal the grain size of the nanocrystalline CoCr coating. The individual “dark spots” indicate grains in the bright-field image as do individual “bright spots” in the dark-field images. The ring pattern in the SAD patterns is typical of nanocrystalline materials. The as-milled powder has an average grain size of 12 nm. After thermal spraying, the resultant coating has an average grain size of 21 nm. This minimal grain growth is not unexpected, considering the particle thermal history during plasma spraying. During the flight from powder feeder to the target, the powder particles are accelerated and heated by the flame, which has a temperature as high as 15,000 K.<sup>8</sup> Under this environment, the feedstock particles (even WC, with a melting point of 3073 K) are usually molten (depending on the particle size) due to the heat transfer from the flame to the particles.<sup>7,20,21</sup> Therefore, it is significant that after such a high-temperature exposure, the grain size remains relatively unchanged (i.e., 21 nm), as compared to the grain size of conventional coatings. Although the grain size of the conventional coating was not determined, based on related studies, a lower boundary on the grain size would be expected to be on the order of tens of microns, based on the starting powder size of 88  $\mu\text{m}$ .<sup>15</sup> The ability to retain a nanometric grain size might be related to the rapid heating during flight and rapid cooling when impinging the substrate. For the spraying distance of 0.1 m used in the present study, the estimated exposure time to the plasma flame is less than  $5 \times 10^{-4}$  s.<sup>28</sup> The short exposure time to high temperature and rapid solidification upon impinging the cold substrate are likely to have limited grain growth in the coating. An additional factor, which might contribute to limited grain growth, is the presence of secondary phases in the milled powders. In a previous study, it was reported that  $\text{Co}_3\text{O}_4$  formed in the milled CoCr powders.<sup>16</sup> In related studies, significant improvements in the thermal stability of nanocrystalline Al alloys have been achieved through the *in situ* formation of fine dispersoids during cryogenic high-energy milling, also known as cryomilling.<sup>17,25</sup> In addition, recent work in this research group has shown that nanoscale dispersoids also exist in cryomilled nanocrystalline Ni (Refs. 11 and 15) and Fe–Al (Ref. 9) powders, generating a thermally stable microstructure. These second-phase particles formed during the mechanical milling process are theorized to impede grain growth through Zener pinning.<sup>9</sup>

Figure 4 shows the corrosion current density of a single conventional and a single nanocrystalline coating for the first sweeping cycle. Only one sample of each

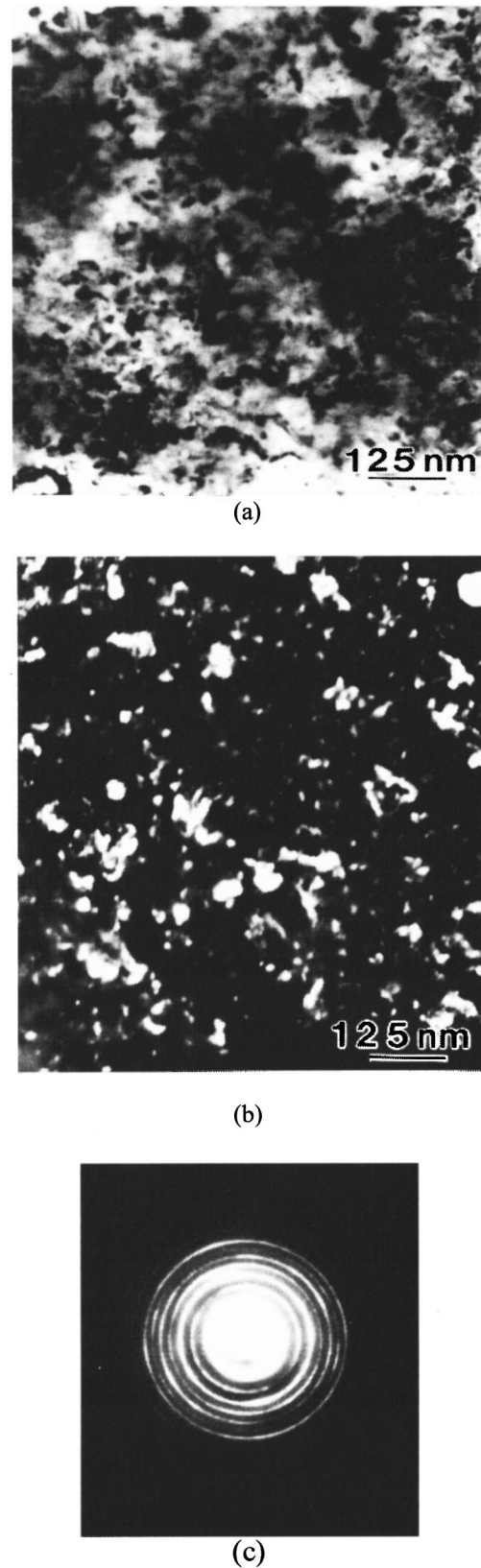
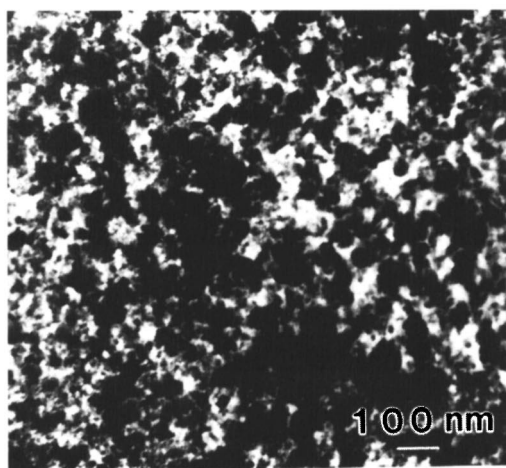
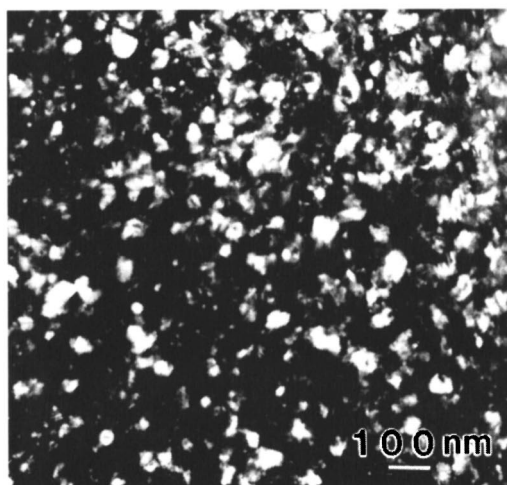


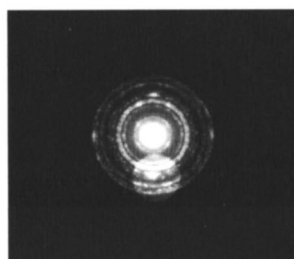
FIGURE 2. TEM bright field (a), dark-field (b), and SAD pattern (c) images of nanocrystalline CoCr powders.



(a)



(b)



(c)

FIGURE 3. TEM bright-field (a), dark-field (b), and SAD pattern (c) images of nanocrystalline CoCr coating.

was tested; however, each sample was put through several hundred cycles to generate Fig. 5. It is apparent that the nanocrystalline coating has a lower corrosion current density ( $\sim 20\%$ ) than that of the conventional coating. Figure 5 shows the current density at 500 and 1500 mV as a function of sweeping cycle. At a lower polarization potential, the current density is low; however, it can still be observed that the nanocrystalline coating is more cor-

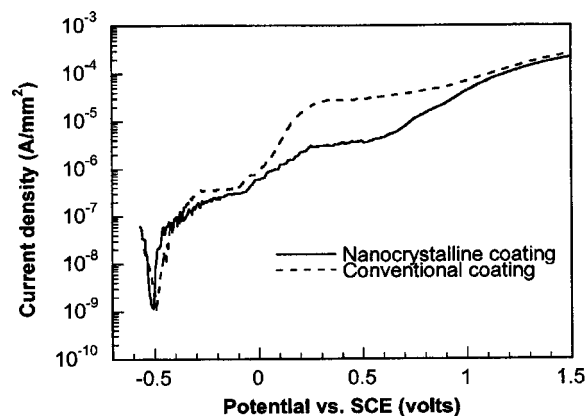


FIGURE 4. Corrosion current density of conventional and nanocrystalline coatings during the first sweeping cycle.

rosion resistant. At a higher potential, this difference is much more obvious. The corrosion current density for the nanocrystalline coating at 1500 mV is about 80% of that of the conventional coating during the entire sweeping test, demonstrating a better corrosion resistance.

The current density shown in Figs. 4 and 5 represents the average dissolution rate of the coating materials. These data alone do not precisely describe the corrosion properties of polycrystalline solids since localized corrosion can lead to premature part failure. In fact, localized degradation is a decisive factor in many component failures caused by a corrosive environment. Hence, to characterize the overall resistance against environmental attack, it is also necessary to assess the degree of localization of corrosion damage. This can be done by SEM surface observation. Figure 6 shows the morphology of the conventional and nanocrystalline coatings after the first sweeping cycle. Large differences can be observed in the corrosion pattern of the different coatings. In the conventional coating, the corrosion appeared to be concentrated at the grain boundaries whereas the interior of the grains remained relatively unchanged. It is

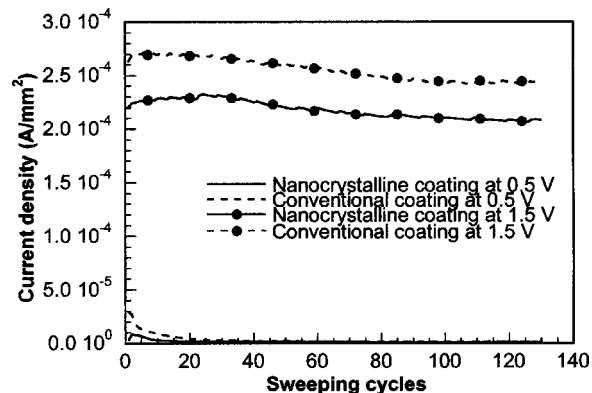
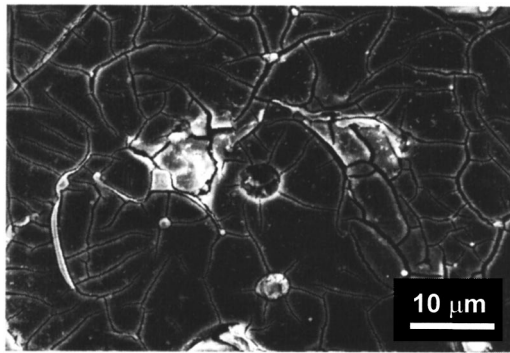
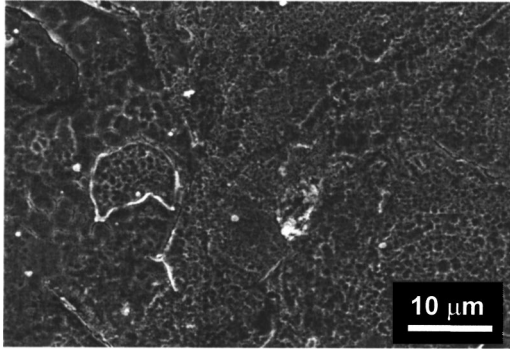


FIGURE 5. Current density at 500 and 1500 mV as a function of sweeping cycle.



(a)



(b)

FIGURE 6. Surface morphology of conventional (a) and nanocrystalline (b) coatings after corrosion test.

important to note that the grain boundary and prior particle boundary are the same for the conventional coating. Also, the large grain size of the conventional coating allows resolution of grains at this magnification, whereas, the grains of the nanocrystalline coating are too small to be resolved by SEM. The intergranular corrosion associated with grain boundaries is considered to be one of the most critical localized damage mechanisms.<sup>1,19,29</sup> For the nanocrystalline coating; however, the corrosion is relatively uniform and no obvious localized corrosion was evident. In a recent study, Vinogradov *et al.* reported that an ultra-fine-grained copper showed a more homogenous corrosion than that of the conventional polycrystalline material.<sup>27</sup> In their report; however, the average corrosion rate of ultrafine copper was reportedly higher than that of the conventional counterpart. The observed lower average corrosion density and corrosive response render the nanocrystalline CoCr coating more attractive for practical applications in comparison with the conventional polycrystalline counterpart; the latter was observed to be susceptible to localized intergranular corrosion.

Inspection of the available scientific literature reveals that there is limited fundamental information on the corrosion mechanisms that are active in nanocrystalline materials. In one of very few studies available, it was

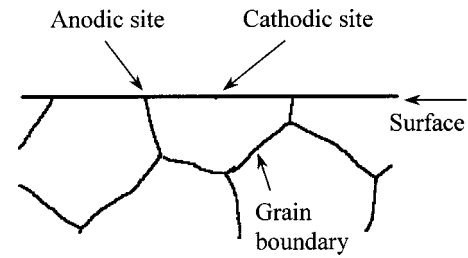


FIGURE 7. Schematic diagram showing grain interior and boundaries as cathodic and anodic sites, respectively.

shown that nanostructured materials produced by electrodeposition may have enhanced corrosion properties in comparison with both their crystalline and amorphous counterparts.<sup>26</sup> Moreover, polarization studies of electrodeposited nanocrystalline Ni (Ref. 22) and Ni–P alloy<sup>23</sup> revealed no improvement or even degradation of corrosion properties. The electrochemical behavior of a mechanically alloyed copper with nanometric grain size has been recently studied.<sup>6</sup> It was found that enhanced corrosion resistance can be achieved in the nanostructured state. The authors attributed this enhancement of corrosion properties to the large fraction of the interface boundaries and argued that with a decrease in grain size, the amount of triple boundaries will increase, which will have the ability to hinder the evolution of a corrosion crack. This interpretation is, however, unlikely because usually grain boundaries significantly facilitate localized dissolution of a material.<sup>1,19,29</sup>

It is well known that the aqueous corrosion of a metal is an electrochemical reaction that requires both oxidation (anodic dissolution) and reduction (cathodic reaction). The anodic and cathodic sites can be characterized by their equilibrium potentials,  $E_a$  and  $E_c$ , respectively. The presence of surface irregularities such as grain boundaries stabilize discrete anodic and cathodic sites so that corrosion is confined to a specific area, i.e., becomes localized. The thermodynamic driving force for corrosion is equal to the difference in equilibrium potentials of anodic and cathodic sites:

$$\Delta E = E_a - E_c. \quad (2)$$

The larger the value of  $\Delta E$ , the higher the corrosion current. It has long been recognized that grain-boundary structure plays a key role in intergranular corrosion mechanisms.<sup>1,19,29</sup> Usually, the grain boundary has a higher energy than the interior of the grain; therefore, it functions as an anodic site while the interior functions as a cathodic site (shown in Fig. 7). The higher the grain-boundary energy, the higher the susceptibility to intergranular damage. Therefore, it is not surprising that in

the conventional CoCr coating, the corrosion occurred primarily in the grain-boundary region.

The role of grain boundaries in nanocrystalline materials on corrosion behavior needs to be addressed carefully, though it is precisely the large amount of grain-boundary area that often promotes many of the unique properties of these materials. An explanation for the enhanced corrosion behavior of the nanocrystalline coating found in this research is not precise at this time; there are three possibilities. The first is that with a decrease in grain size, the atomic compositional difference between the grain interior and the grain boundary caused by atomic segregation is strongly reduced because of the increase in the volume of the grain boundary. Since the equilibrium potential is related to the chemical composition of materials,<sup>2</sup> the decrease in the compositional difference between the grain interior and the grain boundary will result in a decrease in the difference between their equilibrium potentials, leading to a low corrosion rate and a uniform corrosion pattern.

The second factor which might contribute to the observed enhancement in corrosion resistance is the presence of residual strain in nanocrystalline materials.<sup>12</sup> In cryomilled nanocrystalline materials, the grain interior is often heavily deformed; the crystalline lattice is distorted with residual strain. This also may shift the equilibrium potential of the grain interior,  $E_c$ , to the anodic domain, and thus decrease  $\Delta E$ , and consequently, decrease the intergranular dissolution. The third possible explanation for the enhanced corrosion resistance observed in this research is that the high relative grain-boundary-related volume of metal of nanocrystalline materials dramatically influences the repassivation kinetics of these materials.

#### ACKNOWLEDGMENTS

The authors would like to acknowledge the financial support by the Office of Naval Research under Grant No. N00014-94-1-0017. The authors would also like to thank Dr. Stephen M. Jaffe in assistance with computer corrosion data acquisition and Dr. Maggie Lau for her technical contributions.

#### REFERENCES

- <sup>1</sup>Aust, K. T., U. Erb, and G. Palumbo. Interface control for resistance to intergranular cracking. *Mater. Sci. Eng., A* 176:329, 1994.
- <sup>2</sup>Bard, A. J., and L. R. Faulkner. *Electrical Methods: Fundamentals and Applications*. New York: Wiley, 1980, pp. 26–34.
- <sup>3</sup>Birringier, R. Nanocrystalline materials. *Mater. Sci. Eng., A* 117:33–43, 1989.
- <sup>4</sup>Chang, E., W. J. Chang, B. C. Wang, and C. Y. Yang. Plasma spraying of zirconia-reinforced hydroxyapatite composite coatings on titanium. I. Phase, microstructure, and bonding strength. *J. Mater. Sci.: Mater. Med.* 8:193 and 201, 1997.
- <sup>5</sup>Deporter, D. A., P. A. Watson, R. M. Pilliar, M. Pharoah, D. C. Smith, M. Chipman, D. Locker, and A. Rydall. A prospective clinical study in humans of an endosseous dental implant partially covered with a powder-sintered porous coating: 3- to 4-year results. *Int. J. Oral Maxillofac. Implants* 110:87, 1996.
- <sup>6</sup>Elkedim, O., H. S. Cao, C. Meunier, and E. Gaffet. Preparation of nanocrystalline copper by hot and cold compaction: Characterization of mechanical and electrochemical properties. *Mater. Sci. Forum* 843:269–272, 1998.
- <sup>7</sup>Hantzsche, H. In: *Proceedings of the 7th International Metal Spraying Conference*, London, U.K., 10–14 September 1973, Paper No. 16, Abington, Cambridge, England: Welding Institute, 1974.
- <sup>8</sup>Heimann, R. B. *Plasma-Spray Coating: Principles and Applications*. New York: VCH, 1996, p. 19.
- <sup>9</sup>Huang, B., R. J. Perez, and E. J. Lavernia. Grain growth of nanocrystalline Fe–Al alloys produced by cryomilling in liquid argon and nitrogen. *Mater. Sci. Eng., A* 255:124–132, 1998.
- <sup>10</sup>Hulbert, S. F., S. J. Morrison, and J. J. Klawitter. Tissue reaction to three ceramics of porous and nonporous structures. *J. Biomed. Mater. Res.* 6:347, 1972.
- <sup>11</sup>Jiang, H. G., M. L. Lau, and E. J. Lavernia. Grain growth behavior of nanocrystalline Inconel 718 and Ni powder and coatings. *Nanostruct. Mater.* 10:169, 1998.
- <sup>12</sup>Jiang, H., M. Rühle, and E. J. Lavernia. On the applicability of the x-ray diffraction line profile analysis in extracting grain size and microstrain in nanocrystalline materials. *J. Mater. Res.* 14:549, 1999.
- <sup>13</sup>Khor, K. A., C. S. Yip, and P. Cheang. Post-spray hot isostatic pressing of plasma sprayed Ti-6Al-4V/hydroxyapatite composite coatings. *J. Mater. Process. Technol.* 71:280, 1997.
- <sup>14</sup>Klawitter, J. J., and S. F. Hulbert. Application of porous ceramics for the attachment of load bearing internal orthopedic applications. *J. Biomed. Mater. Res. Symp.* 5:61, 1971.
- <sup>15</sup>Lau, M. L., and E. J. Lavernia. Microstructural Evolution and Oxidation Behavior of Spraying. *Mater. Sci. Eng., A* 272:222–229, 1999.
- <sup>16</sup>Lau, M. L., E. Stroock, A. Fabel, C. J. Lavernia, and E. J. Lavernia. In: *Multicomponent Ultrafine Microstructures*, edited by L. E. McCandlish.
- <sup>17</sup>Luton, M. J., C. S. Jayanth, M. M. Disko, S. Matras, and J. Vallone. Synthesis and characterization of nanocrystalline Co–Cr coatings by plasma spraying. *Mater. Res. Soc. Symp. Proc.* 132:79–86, 1989.
- <sup>18</sup>Maniopoulos, C., R. M. Pilliar, and D. C. Smith. Threaded versus porous-surfaced designs for implant stabilization in bone-endodontic implant model. *J. Biomed. Mater. Res.* 20:1309, 1986.
- <sup>19</sup>Mauer, R., U. Erb, and H. Gleiter. Intercrystalline corrosion: Factors controlling the enhanced corrosion near grain boundaries. *Mater. Sci. Eng.* 63:L13, 1984.
- <sup>20</sup>Mishin, J., M. Vardelle, J. Lesinski, and P. Fauchais. Two-colour pyrometer for the statistical measurement of the surface temperature of particles under thermal plasma conditions. *J. Phys. E* 20:620–625, 1987.
- <sup>21</sup>Pawlowski, L. *The Science and Engineering of Thermal Spray Coatings*. New York: Wiley, 1995, p. 86.
- <sup>22</sup>Rofagha, R., R. Langer, A. M. El-Sherik, U. Erb, G. Palumbo, and K. T. Aust. The corrosion behavior of nanocrystalline nickel. *Scr. Metall. Mater.* 25:2867, 1991.
- <sup>23</sup>Rofagha, R., U. Erb, D. Olander, G. Palumbo, and K. T. Aust. The effects of grain size and phosphorous on the cor-

- rosion of nanocrystalline Ni–P alloys. *Nanostruct. Mater.* 2:1, 1993.
- <sup>24</sup>Sobolev, V. V., J. M. Guilemany, and A. J. Martin. In: Proceedings of the 15th International Thermal Spray Conference, edited by C. Coddet. ASM International, Nice, France: ASM International, 1998, Vol. 1, p. 503.
- <sup>25</sup>Tellkamp, V. L., S. Dallek, D. Cheng, and E. J. Lavernia. Grain growth behavior of a nanostructured 5083 Al–Mg alloy. *J. Mater. Res.* 16:938, 2001.
- <sup>26</sup>Thorpe, S. J., B. Ramaswami, and A. T. Aust. Corrosion and Auger studies of a nickel-base metal-metalloid glass. I. The effect of elemental interactions on passivity in the general corrosion of metglass 2826A. *J. Electrochem. Soc.* 135:2162, 1988.
- <sup>27</sup>Vinogradov, A., T. Mimaki, S. Hashimoto, and R. Valiev. On corrosion of ultrafine grained copper produced by equichannel angular pressing. *Mater. Sci. Forum* 312-314:641–646, 1999.
- <sup>28</sup>Westhoff, R., G. Trapaga, and J. Szekely. Plasma–particle interactions in plasma spraying systems. *Metall. Trans. B* 23:683, 1992.
- <sup>29</sup>Yamashita, M., T. Mimaki, S. Hashimoto, and S. Miura. Intergranular corrosion of copper and alpha-Cu–Al alloy bicrystals. *Philos. Mag. A* 63:707, 1991.
- <sup>30</sup>Young, F., M. Spector, and C. H. Kresch. Porous titanium endosseous dental implants in Rhesus monkeys: Microradiography and histological evaluation. *J. Biomed. Mater. Res.* 13:843, 1979.